Pergamon

Int. J. Mech. Sci. Vol. 39, No. 11, pp. 1213–1236, 1997
© 1997 Elsevier Science Ltd
Printed in Great Britain. All rights reserved
0020–7403/97 $17.00 + 0.00

PII: S0020–7403(97)00014–3

MODELLING ONE-DIMENSIONAL UNSTEADY FLOWS IN DUCTS: SYMMETRIC FINITE DIFFERENCE SCHEMES VERSUS GALERKIN DISCONTINUOUS FINITE ELEMENT METHODS

A. ONORATI*, M. PEROTTI* and S. REBAY†

*Department of Energetics, Politecnico of Milano, Piazza L. da Vinci 32, 20133 Milano, Italy,
† Department of Mechanical Engineering, University of Brescia, Via Branze 38, Brescia, Italy

(*Received* 9 *March* 1996; *and in revised form* 24 *September* 1996)

Abstract—The Euler equations for one-dimensional unsteady flows in ducts have been solved resorting to classical symmetric shock-capturing methods with second-order accuracy and to the recent discontinuous Galerkin finite-element method, with second- and third-order accuracy. In particular, the finite difference techniques adopted are the two-step Lax–Wendroff method and the MacCormack predictor–corrector method, with the addition of the flux corrected transport (FCT) or of the Davis nonupwind TVD scheme to suppress the spurious oscillations in the vicinity of discontinuous solutions. The finite-element method adopted is based on the weak formulation of the Euler equations, which are solved by introducing a discontinuous finite-element space discretization. A dissipative mechanism has been considered to supplement the FEM with a "discontinuity capturing" operator, adding a "viscous like" term to damp minor numerical overshoots arising in proximity of steep gradients of the solution. The numerical tests chosen to carry out a comparison between these schemes are the shock-tube problem and the shock–turbulence interaction problem. Both the test cases considered show the superiority of third-order FEM calculations, whereas the comparison between the computer run times points out the greater computational effort required. © 1997 Elsevier Science Ltd.

Keywords: unsteady flows, one-dimensional, numerical methods.

NOTATION

- a speed of sound
- $\mathbf{A}$ anti-diffusion operator
- $\mathbf{C}$ vector of source terms
- d pipe diameter
- $\mathbf{D}$ diffusion operator
- e static internal energy
- e_0 stagnation internal energy
- $\mathbf{F}$ vector of flux terms
- f_w pipe friction factor
- G $= 4f_w u|u|/2d$
- h mesh spacing
- h_0 stagnation enthalpy
- $\mathbf{M}$ mass matrix
- p pressure
- q heat transfer flux per unit mass per unit time
- R specific gas constant
- S cross-sectional area of pipe
- t time
- T temperature
- u gas velocity
- $\mathbf{V}$ test function
- $\mathbf{W}$ vector of conservative variables
- x distance

Greek letters

- ρ density
- Φ diffusive flux
- Ψ anti-diffusive flux
- Ω spatial domain

1. INTRODUCTION

The simulation of one-dimensional unsteady flows in the duct systems of internal combustion engines today certainly plays a fundamental role in design studies of intake and exhaust manifolds, mufflers, valves, etc. Numerical models able to predict the wave motion in the pipes, caused by the periodic charging and discharging process of cylinders, can help the designer to select an optimized geometry of the duct system which ensures the best performances in terms of volumetric efficiency, radiated tailpipe noise, back pressure, and so on. The experimental work on the engine may be drastically reduced to that of testing and refining a few possible configurations previously selected by means of the predictive tools. Several computer codes have been developed for this purpose in the last decade, based on the numerical solution of the conservation equations for 1D unsteady flows through different numerical techniques. Surely the mesh method of characteristics has been the most widely used in this field, due to the extensive research work carried out during the last three decades [1–3]. However, several drawbacks of this technique have been stressed, such as the low accuracy (first order) and the poor resolution of shocks (both due to linear interpolation between two nodes), the cumbersome use of path lines to solve the non-homentropic problem and the difficult extension to treat mixtures of gases with different composition and specific heats variable with temperature. These limitations have induced the researchers to devise and adopt more robust high-resolution schemes to solve the non-linear hyperbolic problem in conservation form.

In recent years, on one hand classical symmetric (non-upwind) shock-capturing schemes with second-order accuracy have been introduced in simulation models, such as the two-step Lax–Wendroff and the MacCormack methods [4–6]; on the other hand, characteristic-based (upwind) TVD (total variation diminishing) and ENO (essentially non-oscillatory) schemes have been adopted [7].

The former family of finite-difference methods undoubtedly offers a great simplicity, since the same shock-capturing algorithm, independently of the local pattern of characteristic lines, may be applied in each node of the grid. No exact or approximate Riemann solver is required. Thus very fast and efficient computation techniques may be implemented (about three times faster than the mesh method of characteristics). The typical problem of numerical overshoots around shock waves and contact surfaces has been solved resorting to flux-corrected transport in different forms (FCT) [8–10] and to non-upwind TVD schemes [11], both based on non-linear flux limiters to determine the proper amount of artificial viscosity to eliminate local instabilities. Moreover, these methods can be directly applied to the calculation of wave motion in gases with variable composition and specific heats [12, 13]. The disadvantage of this approach, which does not exploit the information inherent in the characteristic lines, is the smearing of discontinuous solutions, so that shocks and contact surfaces are captured within a few mesh points. Furthermore, high-frequency oscillations of fluid dynamic variables may be not properly captured, if the grid is not significantly refined. Finally, schemes with accuracy of third order (or more) may be arranged by widening the stencil which creates some problems when dealing with the boundary conditions.

The family of methods using characteristic-based techniques allows a better definition of discontinuous solutions, biasing the scheme according to the direction of the propagation of the information. Second-order numerical schemes have been devised by using exact or approximate Riemann solvers to introduce the upwinding, and appropriate limiting techniques to prevent the formation of spurious oscillations [7, 14]. Higher-order schemes can be constructed resorting to wider stencils. The advantages of these methods are the excellent capturing of shocks and contact discontinuities, which are generally localized within a couple of grid cells. Minor drawbacks are represented by the complexity of both the algorithms and the implementation, the increased computational effort compared to symmetric schemes and the computational cost of Reimann solvers for real gases [15] when the assumption that the fluid is a perfect gas is removed.

Recently a new class of numerical schemes has been considered [16, 17] to solve hyperbolic problems, on the basis of the discontinuous Galerkin finite element method. This variational approach [18] for the solution of conservation laws offers the advantage of a more general theoretical framework, which allows the application of the method to unstructured grids in multidimensional problems, unlike finite-difference upwind schemes, whose extension to unstructured grids is rather complex. Piecewise discontinuous polynomials are used as basis functions to approximate the solution inside the elements, and Riemann solvers are employed to evaluate

numerical fluxes at element interfaces. This numerical method is particularly flexible, in that it allows the construction of high-order numerical schemes simply by raising the order of the approximating polynomials inside the elements. It is important to point out that high-order discontinuous finite-element schemes are obtained with no need of wide stencils. This property is essential when dealing with the boundary conditions, which can be treated in a very natural way.

The aim of this paper is to present a detailed comparison between the new highly accurate discontinuous Galerkin finite-element method and the classical symmetric shock-capturing schemes. In particular, the two-step Lax–Wendroff method (LW2) and the MacCormack method (MCK) (with flux-corrected transport (FCT) or with a non-upwind TVD algorithm to suppress numerical overshoots) have been considered. The outline of the finite-difference techniques and the general theory and algorithms of the discontinuous Galerkin method are reported in the paper. The calculated solutions of two typical numerical tests, i.e. the shock-tube problem and the shock-turbulence interaction, have been investigated and compared, on the basis of the accuracy of the solution and of the computational efforts.

2. SYMMETRIC FINITE-DIFFERENCE SCHEMES

The general approach to modelling the wave action in engine intake and exhaust pipe systems is based on the numerical solution of the conservation laws for a one-dimensional, unsteady, compressible flow. Basically, these are the Euler equations (continuity, momentum, energy) with addition of source terms accounting for pipe cross-sectional area variations, friction and heat transfer at duct walls. The resulting quasi-linear hyperbolic problem may be written in conservative form:

$$\frac{\partial \mathbf{W}}{\partial t} + \frac{\partial \mathbf{F}(\mathbf{W})}{\partial x} + \mathbf{C}(\mathbf{W}) = 0 \tag{1}$$

where

$$\mathbf{W}(x,t) = \begin{bmatrix} \rho \\ \rho u \\ \rho e_0 \end{bmatrix}, \quad \mathbf{F}(\mathbf{W}) = \begin{bmatrix} \rho u \\ \rho u^2 + p \\ \rho u h_0 \end{bmatrix}, \quad \mathbf{C}(\mathbf{W}) = \begin{bmatrix} \rho u \\ \rho u^2 \\ \rho u h_0 \end{bmatrix}, \frac{1}{S}\frac{\mathrm{d}S}{\mathrm{d}x} + \begin{bmatrix} 0 \\ \rho G \\ -\rho q \end{bmatrix} \tag{2}$$

are the conserved variable, the flux and the source term vectors, respectively (x, t are distance and time co-ordinates; p, u, ρ, e_0, h_0 are pressure, flow velocity, density, stagnation specific internal energy and enthalpy, respectively; S is the cross-sectional area, $G = 4f_w u|u|/2d$, d is the duct diameter, f_w is the friction factor at the duct wall, q is the heat transfer energy per unit mass per unit time). The thermodynamic behaviour of the fluid must be expressed by an equation of state, which is necessary to close the problem: the most common assumption is to consider a perfect gas with constant specific heats ($p/\rho = RT$, $c_p/c_v = \text{const.}$) and constant composition. However, more general assumptions may be introduced, to allow for mixtures of ideal gases with c_p/c_v as a function of temperature T and chemical composition [12, 13]. This is fundamental to cope with the calculation of the wave motion in hot exhaust gases of i.c. engines.

Efficient symmetric shock-capturing schemes may be employed for the solution of the hyperbolic problem in conservation form. In particular, in the last decade the classical two-step Lax–Wendroff method and the MacCormack predictor–corrector method have been implemented in different numerical codes [6, 19, 20], achieving a reasonable compromise between accuracy, resolution of discontinuities, simplicity and computational time. More recently, the new space–time conservation element-solution element method [21], an innovative symmetric finite-difference scheme, has been applied to the simulation of unsteady flows in engine ducts [22, 23]. A concise description of the Lax–Wendroff method, the MacCormack method and the FCT and TVD techniques is reported in what follows [18].

First of all, both methods are non-upwinded, shock capturing and explicit in time, with second-order accuracy ($O(\Delta x^2, \Delta t^2)$) and are able to capture sharp discontinuities in the flow field (shock waves or contact discontinuities). Being symmetric, they adopt the same finite difference scheme in every calculation point, without requiring any information about the local characteristic lines.

The two-step Lax–Wendroff method (LW2) calculates the solution vector $\mathbf{W}^{n+1}$ at time t_{n+1} in the node i from the known vectors $\mathbf{W}^n$, $\mathbf{F}^n$, $\mathbf{C}^n$ in the nodes $i-1$, i, $i+1$ (three-point stencil) at time

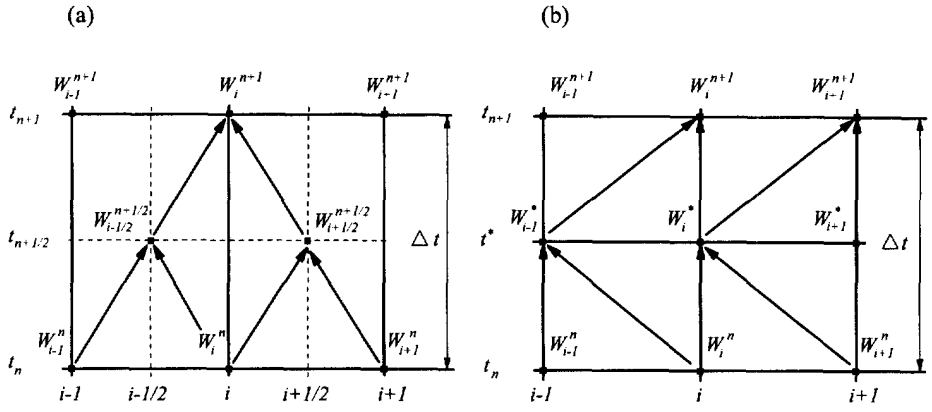

Fig. 1. Distance–time plane for the two-step Lax–Wendroff method (a) and the MacCormack predictor–corrector method (b).

t_n, by means of two steps [Fig. 1(a)]. In the first step, $\mathbf{W}^{n+1/2}$ is computed in the intermediate nodes $i - 1/2$, $i + 1/2$ at time $t_{n+1/2}$ (forward in time of $\Delta t/2$):

$$\mathbf{W}_{i+1/2}^{n+1/2} = \tfrac{1}{2}(\mathbf{W}_{i+1}^n + \mathbf{W}_i^n) - \frac{\Delta t}{2\Delta x}(\mathbf{F}_{i+1}^n - \mathbf{F}_i^n) - \frac{\Delta t}{4}(\mathbf{C}_{i+1}^n + \mathbf{C}_i^n)$$
$$\mathbf{W}_{i-1/2}^{n+1/2} = \tfrac{1}{2}(\mathbf{W}_i^n + \mathbf{W}_{i-1}^n) - \frac{\Delta t}{2\Delta x}(\mathbf{F}_i^n - \mathbf{F}_{i-1}^n) - \frac{\Delta t}{4}(\mathbf{C}_i^n + \mathbf{C}_{i-1}^n). \tag{3}$$

Having evaluated the vector $\mathbf{W}^{n+1/2}$ in the half-way points $i + 1/2$, $i - 1/2$, the vectors $\mathbf{F}^{n+1/2}(\mathbf{W})$, $\mathbf{C}^{n+1/2}(\mathbf{W})$ may be calculated in the same positions. This first step to the intermediate time level $t_n + \Delta t/2$ avoids the cumbersome computation of the Jacobian matrix $\mathbf{J} = \partial\mathbf{F}/\partial\mathbf{W}$, essential in the one-step Lax–Wendroff method. With a second step, the solution vector $\mathbf{W}^{n+1}$ at t_{n+1} is evaluated on the basis of the known vectors $\mathbf{F}^{n+1/2}$, $\mathbf{C}^{n+1/2}$ in the half-way nodes $i - 1/2$, $i + 1/2$:

$$\mathbf{W}_i^{n+1} = \mathbf{W}_i^n - \frac{\Delta t}{\Delta x}(\mathbf{F}_{i+1/2}^{n+1/2} - \mathbf{F}_{i-1/2}^{n+1/2}) - \frac{\Delta t}{2}(\mathbf{C}_{i+1/2}^{n+1/2} + \mathbf{C}_{i-1/2}^{n+1/2}). \tag{4}$$

Similarly, the MacCormack method (MCK) is based on two steps on a three-point stencil. A provisional solution vector $\mathbf{W}^*$ is evaluated by a predictor step [forward differences, Fig. 1(b)] at the time t^*, on the basis of the known vector $\mathbf{W}^n$, $\mathbf{F}^n$, $\mathbf{C}^n$:

$$\mathbf{W}_i^* = \mathbf{W}_i^n - \frac{\Delta t}{\Delta x}(\mathbf{F}_{i+1}^n - \mathbf{F}_i^n) - \Delta t\,\mathbf{C}_i^n. \tag{5}$$

$\mathbf{W}_i^*$ is then used to calculate the corresponding vectors $\mathbf{F}_i^*$, $\mathbf{C}_i^*$. The solution vector $\mathbf{W}^{n+1}$ is finally achieved by a corrector step (backward differences):

$$\mathbf{W}_i^{n+1} = \frac{1}{2}\left[\mathbf{W}_i^n + \mathbf{W}_i^* - \frac{\Delta t}{\Delta x}(\mathbf{F}_i^* - \mathbf{F}_{i-1}^*) - \Delta t\,\mathbf{C}_i^*\right]. \tag{6}$$

In order to achieve the best results in calculating discontinuous solutions, it has been suggested to reverse the orientation of finite differences at each time step (backward predictor–forward corrector at time t_k, forward predictor–backward corrector at time t_{k+1}, and so on).

The time increment Δt is regulated by the Courant–Fredrichs–Lewy criterion in both methods, which state

$$\mathrm{CFL} = (a + |u|)\frac{\Delta t}{\Delta x} \leqslant 1 \tag{7}$$

for the stability of the calculation, where a is the sound speed and u the gas velocity.

The typical problem of second- (or higher-) order shock-capturing schemes, i.e. the inevitable presence of spurious overshoots in the proximity of discontinuities, may be summarized as follows.

Every second- (or higher-) order unwinded or centered numerical scheme of the form

$$\mathbf{W}_i^{n+1} = \sum_k c_k \mathbf{W}_{i+k}^n \tag{8}$$

with constant coefficients c_k (linear scheme) is not TVD (total variation diminishing), according to the well-known Godunov's theorem, as reported in Ref. [16]. It means that the total variation (TV) of the numerical solution, defined by

$$\mathrm{TV}[\mathbf{W}_i^n] = \sum_i |\mathbf{W}_{i+1}^n - \mathbf{W}_i^n| \tag{9}$$

does not respect the condition

$$\mathrm{TV}[\mathbf{W}^{n+1}] \leqslant \mathrm{TV}[\mathbf{W}^n] \tag{10}$$

which ensures the attainment of a monotonic solution. This results in the production of local instabilities in the solution near discontinuities. To satisfy the above requirement, the scheme needs coefficients c_k which depend on the values of $\mathbf{W}^n$ (non-linear scheme).

Different numerical algorithms have been developed in the past to mitigate or eliminate the spurious oscillations in the solution. In the present work the flux-corrected-transport (FCT) technique of Boris and Book [8, 9] via smoothing and via damping, and the non-upwind total variation diminishing (TVD) algorithm by Davis [11] have been considered and implemented. A detailed description of both techniques is given in [4, 13, 20, 24], whereas a brief introduction to the non-upwind TVD scheme is reported below.

The total variation diminishing (TVD) algorithm devised by Davis [11] in a non-upwind form provides a non-linear term to be appended to the solution vector $\mathbf{W}$, calculated by the Lax–Wendroff and MacCormack schemes, in order to achieve a monotonic solution. The proper amount of artificial viscosity, to be introduced in each node to avoid the occurrence of numerical overshoots, is determined by means of a suitable flux limiter.

The term to be appended is given by

$$[G_i^+ + G_{i+1}^-]\Delta\mathbf{W}_{i+1/2}^n - [G_{i-1}^+ + G_i^-]\Delta\mathbf{W}_{i-1/2}^n \tag{11}$$

where

$$\begin{aligned} \Delta\mathbf{W}_{i+1/2}^n &= \mathbf{W}_{i+1}^n - \mathbf{W}_i^n \\ \Delta\mathbf{W}_{i-1/2}^n &= \mathbf{W}_i^n - \mathbf{W}_{i-1}^n \end{aligned} \tag{12}$$

and

$$G_i^{\pm} = G(r_i^{\pm}) = 0.5C(v)[1 - \hat{\phi}(r_i^{\pm})] \tag{13}$$

with

$$C(v) = \begin{cases} v(1-v), & v \leqslant 0.5 \\ 0.25, & v > 0.5 \end{cases} \qquad v = v_i = \max|\lambda|\frac{\Delta t}{\Delta x} \quad (\max|\lambda| = |u| + a) \tag{14}$$

while the flux limiter

$$\hat{\phi}(r) = \begin{cases} \min(2r, 1), & r > 0 \\ 0, & r \leqslant 0 \end{cases} \tag{15}$$

controls the employment of the artificial viscosity in each node. The values $r_i^{\pm}$ are calculated on the basis of $\mathbf{W}^n$ as follows:

$$\begin{aligned} r_i^+ &= \frac{[\Delta\mathbf{W}_{i-1/2}^n, \Delta\mathbf{W}_{i+1/2}^n]}{[\Delta\mathbf{W}_{i+1/2}^n, \Delta\mathbf{W}_{i+1/2}^n]} \\ r_i^- &= \frac{[\Delta\mathbf{W}_{i-1/2}^n, \Delta\mathbf{W}_{i+1/2}^n]}{[\Delta\mathbf{W}_{i-1/2}^n, \Delta\mathbf{W}_{i-1/2}^n]} \end{aligned} \tag{16}$$

where $[.,.]$ represents the scalar product of the vectors contained in the square brackets.

By appending the term (20) to the solution vector $\mathbf{W}$ a complete elimination of spurious oscillations can be achieved. As suggested in Ref. [13], a reduction of the *CFL* number to 0.7 is required for the numerical stability of the scheme.

Moreover, Harten's artificial compression (AC) method [25] has been implemented, to be eventually appended to the TVD technique. The AC technique can be used to improve the definition of sharp gradients in the solution (due to shock waves and contact discontinuities) when they occur. Briefly, the artificial compression operator $\mathbf{C}_\Delta$ is defined by

$$\mathbf{C}_\Delta \mathbf{W}_i = \mathbf{W}_i - \frac{\omega}{2}[\theta_{i+1/2}\mathbf{G}_{i+1/2} - \theta_{i-1/2}\mathbf{G}_{i-1/2}] \tag{17}$$

where $\mathbf{C}_\Delta \mathbf{W}_i$ is the solution vector after the application of the AC, whilst $\mathbf{W}_i$ is the solution given by the numerical method plus the TVD algorithm. Moreover, θ and $\mathbf{G}$ are defined as follows:

$$\theta_{i+1/2} = \max[\hat{\theta}_i, \hat{\theta}_{i+1}] \tag{18}$$

$$\hat{\theta}_i = \begin{cases} \left| \dfrac{|\Delta\rho_{i+1/2}| - |\Delta\rho_{i-1/2}|}{|\Delta\rho_{i+1/2}| + |\Delta\rho_{i-1/2}|} \right|, & |\Delta\rho_{i+1/2}| + |\Delta\rho_{i-1/2}| > \varepsilon \\ 0, & |\Delta\rho_{i+1/2}| + |\Delta\rho_{i-1/2}| \leqslant \varepsilon \end{cases} \tag{19}$$

$$\varepsilon = \delta \max_i |\rho_{i+1} - \rho_i| \tag{20}$$

$$\mathbf{G}_{i+1/2} = G^m_{i+1/2} = g^m_i + g^m_{i+1} - |g^m_{i+1} - g^m_i| \operatorname{sgn}[W^m_{i+1} - W^m_i] \tag{21}$$

$$g^m_i = \alpha_i(W)[W^m_{i+1} - W^m_{i-1}] \tag{22}$$

$$\alpha_i(W) = \max\left[0, \min_{1 \leqslant m \leqslant M} \frac{\min[|W^m_{i+1} - W^m_i|, [W^m_i - W^m_{i-1}] \operatorname{sgn}[W^m_{i+1} - W^m_i]]}{|W^m_{i+1} - W^m_i| + |W^m_i - W^m_{i-1}|}\right], \tag{23}$$

with M equal to the number of components of the vector $\mathbf{W}$ and the parameter ω set to 1.0.

It may be noted that the parameter $\hat{\theta}_i$ regulates the action of artificial compression in different regions of the solution; when the sum of adjacent density differences given in Eqn (19) is greater than the tolerance parameter ε, then $\hat{\theta}_i$ is greater than zero and the gradient of the solution is increased. The tolerance ε depends on the parameter δ, which is problem dependent; it has been set to 0.75 in this work, as suggested in Ref. [13].

3. DISCONTINUOUS GALERKIN FORMULATION

We now consider the numerical solution of the Euler equations (1) by means of a discontinuous finite element Galerkin method (discontinuous FEM), which is based on a discontinuous finite element space discretization originally considered for the solution of the neutron transport equation by Lesaint and Raviart [26, 27] and more recently refined by Cockburn and Shu [16, 17] for the solution of non-linear systems of conservation laws. This method has been applied successfully to 1D shock-tube problems and to the numerical simulation of 2D inviscid and viscous transonic flows over airfoils in [28, 29, 30].

The weak formulation of the Euler equations is obtained by integrating, over the spatial domain $\Omega = (a, b)$, the product of the Euler equations in differential form with a test function $\mathbf{V}(x)$ and by performing an integration by parts of the integrals containing the derivative of the flux function. The weak form of the Euler equation is, therefore,

$$\int_a^b \mathbf{V} \frac{\partial \mathbf{W}}{\partial t}\, dx + [\mathbf{V}\mathbf{F}(\mathbf{W})]_a^b - \int_a^b \frac{d\mathbf{V}}{dx}\mathbf{F}(\mathbf{W})\, dx = -\int_a^b \mathbf{V}\mathbf{C}(\mathbf{W})\, dx \quad \forall\, \mathbf{V}. \tag{24}$$

A discrete analogue of Eqn (24) is obtained by subdividing the domain Ω into a collection of non-overlapping elements $E_i = \{x \in \Re: x_i \leqslant x \leqslant x_{i+1}\}$, $i = 1, 2, \ldots, N$ of uniform length $h = x_{i+1} - x_i$ and by considering functions $\mathbf{W}_h$ and $\mathbf{V}_h$ which are polynomials P^k of degree less than

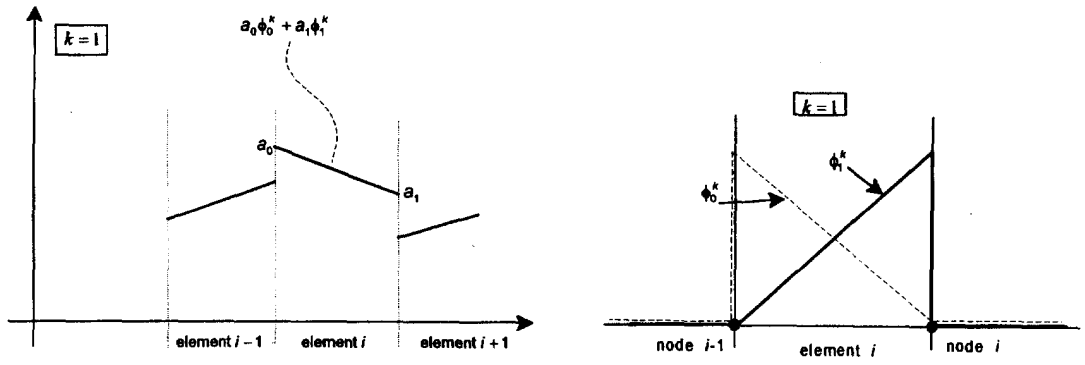

(a) (b)

$$\begin{bmatrix} \int_{x_i}^{x_{i+1}} \phi_0^1\phi_0^1\,dx & 0 & 0 & \int_{x_i}^{x_{i+1}} \phi_0^1\phi_1^1\,dx & 0 & 0 \\ 0 & \int_{x_i}^{x_{i+1}} \phi_0^1\phi_0^1\,dx & 0 & 0 & \int_{x_i}^{x_{i+1}} \phi_0^1\phi_1^1\,dx & 0 \\ 0 & 0 & \int_{x_i}^{x_{i+1}} \phi_0^1\phi_0^1\,dx & 0 & 0 & \int_{x_i}^{x_{i+1}} \phi_0^1\phi_1^1\,dx \\ \int_{x_i}^{x_{i+1}} \phi_1^1\phi_0^1\,dx & 0 & 0 & \int_{x_i}^{x_{i+1}} \phi_1^1\phi_1^1\,dx & 0 & 0 \\ 0 & \int_{x_i}^{x_{i+1}} \phi_1^1\phi_0^1\,dx & 0 & 0 & \int_{x_i}^{x_{i+1}} \phi_1^1\phi_1^1\,dx & 0 \\ 0 & 0 & \int_{x_i}^{x_{i+1}} \phi_1^1\phi_0^1\,dx & 0 & 0 & \int_{x_i}^{x_{i+1}} \phi_1^1\phi_1^1\,dx \end{bmatrix} \begin{bmatrix} \frac{d\hat{w}_{01}}{dt} \\ \frac{d\hat{w}_{02}}{dt} \\ \frac{d\hat{w}_{03}}{dt} \\ \frac{d\hat{w}_{11}}{dt} \\ \frac{d\hat{w}_{12}}{dt} \\ \frac{d\hat{w}_{13}}{dt} \end{bmatrix} \begin{matrix} \} \frac{d\hat{\mathbf{W}}_1}{dt} \\ \\ \\ \} \frac{d\hat{\mathbf{W}}_2}{dt} \\ \\ \end{matrix}$$

where $\hat{\mathbf{W}}_l = [\hat{w}_{l1} \quad \hat{w}_{l2} \quad \hat{w}_{l3}]^T = [\hat{\rho} \quad \hat{\rho u} \quad \hat{\rho e}_{0l}]^T$

(c)

Fig. 2. Piecewise linear approximation (a) and piecewise linear shape functions (b) within element i; structure of the first term of Eqn (27) with $k = 1$ (c).

or equal to k within each element (Galerkin method). The functions $\mathbf{W}_h$ and $\mathbf{V}_h$ can be written in general as

$$\mathbf{W}_h(x,t)|_{E_i} = \sum_{l=0}^{k} \hat{\mathbf{W}}_l(t)\phi_l^k(x), \quad \mathbf{V}_h(x)|_{E_i} = \sum_{j=0}^{k} \hat{\mathbf{V}}_j\phi_l^k(x), \quad \forall x \in E_i \tag{25}$$

where the expansion coefficients $\hat{\mathbf{W}}_l(t)$ and $\hat{\mathbf{V}}_j$ denote the degrees of freedom of the numerical solution and of the test function within the element E_i, respectively, and the shape functions ϕ_j^k are a base for the polynomial functions P^k. Note that there is no global continuity requirement for $\mathbf{W}_h$ and $\mathbf{V}_h$, which are therefore discontinuous functions across element interfaces [Fig. 2(a)]. Moreover, the order of accuracy in space is given by $O(h^{k+1})$; so, for example, we have second-order accuracy when using linear elements, i.e. $k = 1$.

By regarding the integral over Ω as the sum of integrals over the elements E_i, and by considering the functions $\mathbf{W}_h$ and $\mathbf{V}_h$, we obtain the semidiscrete equations for a generic element E_i:

$$\frac{\mathrm{d}}{\mathrm{d}t}\int_{x_i}^{x_{i+1}} \mathbf{V}_h\mathbf{W}_h\,\mathrm{d}x + [\mathbf{V}_h\mathbf{F}(\mathbf{W}_h)]_{x_i}^{x_{i+1}} - \int_{x_i}^{x_{i+1}} \frac{\mathrm{d}\mathbf{V}_h}{\mathrm{d}x}\mathbf{F}(\mathbf{W}_h)\,\mathrm{d}x + \int_{x_i}^{x_{i-1}} \mathbf{V}_h\mathbf{C}(\mathbf{W}_h)\,\mathrm{d}x = 0 \quad \forall\, \mathbf{V}_h. \tag{26}$$

Equation (26) must be satisfied for any element E_i and for *any* function $\mathbf{V}_h$, that means for any value $\mathbf{V}_j$ according to Eqn (25) (see Fig. 2). Hence, in Eqn (26) $\mathbf{V}_h$ may be taken as $\phi_0^k, \phi_1^k, \ldots, \phi_k^k$ in

sequence. As a consequence, taking into account also the definition of $\mathbf{W}_h$ (25), Eqn (26) is equivalent to a system of $k+1$ vector equations:

$$\frac{\mathrm{d}}{\mathrm{d}t}\int_{x_i}^{x_{i+1}} \phi_j^k \phi_l^k \hat{\mathbf{W}}_l \,\mathrm{d}x + [\phi_j^k \mathbf{F}(\mathbf{W}_h)]_{x_i}^{x_{i+1}} - \int_{x_i}^{x_{i+1}} \frac{\mathrm{d}\phi_j^k}{\mathrm{d}x}\mathbf{F}(\mathbf{W}_h)\,\mathrm{d}x + \int_{x_i}^{x_{i+1}} \phi_j^k \mathbf{C}(\mathbf{W}_h)\,\mathrm{d}x = 0 \quad 0 \leqslant j,l \leqslant k \tag{27}$$

which are sufficient to determine the $k+1$ degrees of freedom $\hat{\mathbf{W}}_l(t)$ of the unknown solution $\mathbf{W}_h$ inside the element E_i. Since the shape functions have been chosen so that $\phi_j^k(x) = \phi_l^k(x) = 0$ $\forall\, x \notin E_i$, the (mass) matrix $M_{j,l} = \int_{x_i}^{x_{i+1}} \phi_j^k \phi_l^k \,\mathrm{d}x$ couples the $k+1$ degrees of freedom within one element only. The structure of the mass matrix is shown in detail for $k=1$ in Fig. 2(c).

Due to the discontinuous approximation of the unknowns, the interface flux functions $\mathbf{F}(\mathbf{W}_h)_i$ and $\mathbf{F}(\mathbf{W}_h)_{i+1}$ appearing in the second term of Eqn (27) are not uniquely defined. It is at this stage that the technique traditionally used in finite-volume schemes is borrowed by the discontinuous finite-element method. The flux functions appearing in the second term of Eqn (27) are in fact replaced by a numerical flux function $\mathbf{H}(\mathbf{W}_h^-, \mathbf{W}_h^+)$ which depends on the internal interface state $\mathbf{W}_h^+$ and on the neighbouring element interface state $\mathbf{W}_h^-$. In order to guarantee the formal accuracy of the scheme, $\mathbf{H}(\mathbf{W}_h^-, \mathbf{W}_h^+)$ is required to satisfy the relations [16]:

$$\mathbf{H}(\mathbf{W},\mathbf{W}) = \mathbf{F}(\mathbf{W}), \quad \mathbf{H}(\mathbf{W},\mathbf{Y}) = -\mathbf{H}(\mathbf{Y},\mathbf{W}) \tag{28}$$

(where $\mathbf{Y}$ is a generic vector) which are called the consistency condition and the directional consistency condition, respectively. Among the many numerical flux functions which satisfy the consistency criteria and can be used to evaluate the interface state using the information coming from the "upwind" interface element, we have used the exact (Godunov) Riemann flux function.

The method described so far, despite the upwind treatment of the fluxes at the element interfaces, amounts to a linear higher-order scheme which introduces oscillations if the flow discontinuities are not located exactly at the element interfaces. In order to compute physically relevant solutions without oscillations, it is therefore necessary to augment the discontinuous finite-element method with some dissipative mechanism which does not destroy the formal order of accuracy of the scheme, such as the local projection limiting strategy proposed by Cockburn and Shu [16]. In the present work, however, we use a different approach [31] which consists of supplementing the FEM with a "discontinuity capturing" operator similar to that commonly considered in the streamline upwind Petrov–Galerkin (SUPG) finite element method [32]. In practice, we add to the left-hand side of Eqn (27) a "viscous-like" term

$$\int_{x_i}^{x_{i+1}} \frac{\mathrm{d}\phi_i^k}{\mathrm{d}x}\,\varepsilon\,\frac{\partial \mathbf{W}_h}{\partial x}\,\mathrm{d}x \tag{29}$$

where the scalar coefficient ε is a constant value within each element given by

$$\varepsilon = Kh^2 \left\{ \sum_{m=1}^{M} [(|\bar{W}_{h_m}| + c)^{-1} \bar{R}_{E_m}(\mathbf{W}_h)]^2 \right\}^{1/2}. \tag{30}$$

In this equation K and c are positive parameters, h is the mesh spacing, M is the number of components of the vector $\mathbf{W}$, $\bar{W}_{h_m}$ is the mth component of the average vector $\bar{\mathbf{W}}_h$ within the element of $\bar{R}_{E_m}$ is the mth component of the average residual vector $\bar{\mathbf{R}}_E$ given by

$$\bar{\mathbf{R}}_E(\mathbf{W}_h) = \frac{1}{h}\int_{x_i}^{x_{i+1}} \left[\frac{\partial \mathbf{W}_h}{\partial t} + \frac{\partial \mathbf{F}(\mathbf{W}_h)}{\partial x} + \mathbf{C}(\mathbf{W}_h)\right]\mathrm{d}x. \tag{31}$$

The parameter K controls the amount of dissipation added to the scheme and c is a small constant needed to avoid division by zero when $|\bar{W}_{h_m}| = 0$; c has been set equal to h in our calculations. It should be noted that the amount of dissipation introduced by Eqn (30) is proportional to the residual of the equations and is therefore vanishingly small when the numerical solution $\mathbf{W}_h$ satisfies to the Euler equations.

Interesting features of this artificial viscosity operator are that no problem-dependent fine tuning is needed, since the proper K values to be adopted seem to depend only on the order of the FEM, and may be optimized on the basis of test cases for a general use, as it will be shown in the next section.

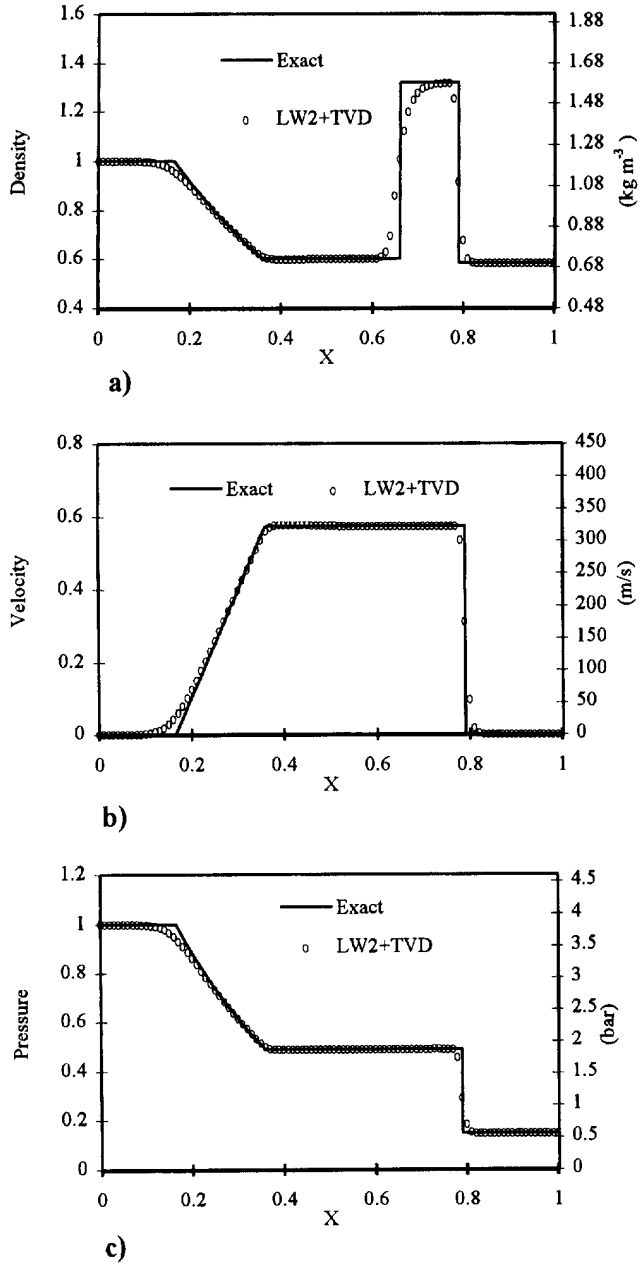

Fig. 3. Results of the shock-tube problem using the Lax–Wendroff method plus TVD.

All the integrals appearing in Eqn (27) and the discontinuity capturing operator are evaluated by means of Gauss numerical quadrature formulae with a number of integration points consistent with the accuracy required. By assembling together all the elemental contributions given by Eqn (27), the system of ordinary differential equations which govern the evolution in time of the discrete solution can be written as

$$\mathbf{M}\frac{\mathrm{d}\hat{\hat{\mathbf{W}}}}{\mathrm{d}t} + \mathbf{R}(\hat{\hat{\mathbf{W}}}) = \mathbf{0} \tag{32}$$

where $\mathbf{M}$ denotes the global mass matrix, $\hat{\hat{\mathbf{W}}}$ the global vector of the degrees of freedom, and $\mathbf{R}(\hat{\hat{\mathbf{W}}})$ the global residual vector, which includes the second, third and forth terms of Eqn (27). The matrix $\mathbf{M}$ assumes a block diagonal structure by a suitable manipulation so that the time integration of this

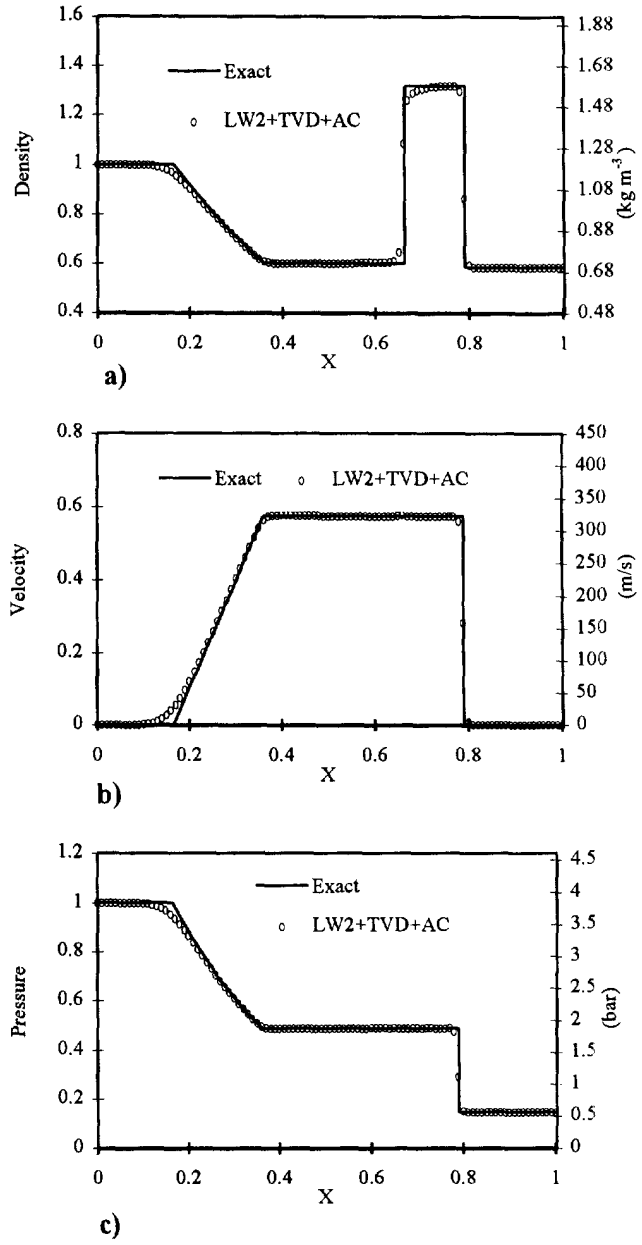

Fig. 4. Results of the shock-tube problem using the Lax–Wendroff method plus TVD and AC.

system can be accomplished in a very efficient way by means of a Runge–Kutta explicit method for initial-value problems. In order to attain the same accuracy in time as in space, i.e. $O(h^{k+1}, \Delta t^{k+1})$, in this work the semidiscrete equations obtained with linear ($k = 1$) and quadratic ($k = 2$) elements have been marched forward in time with the two- and three-stage Runge–Kutta methods, to guarantee second- and third-order time accuracy, respectively, as suggested by Cockburn and Shu in Ref. [16]. In this case the scheme is proved to be linearly stable under the condition CFL $\leqslant 1/(2k + 1)$, as shown in Ref. [16], where k is the order of the shape functions ϕ_j^k and $k + 1$ is the order of accuracy of the numerical method.

4. NUMERICAL RESULTS

Here we present the results of computations with the above methods for two common test cases. Calculations were performed on a HP 735/125 MHz computer in double precision (64 bits per floating point).

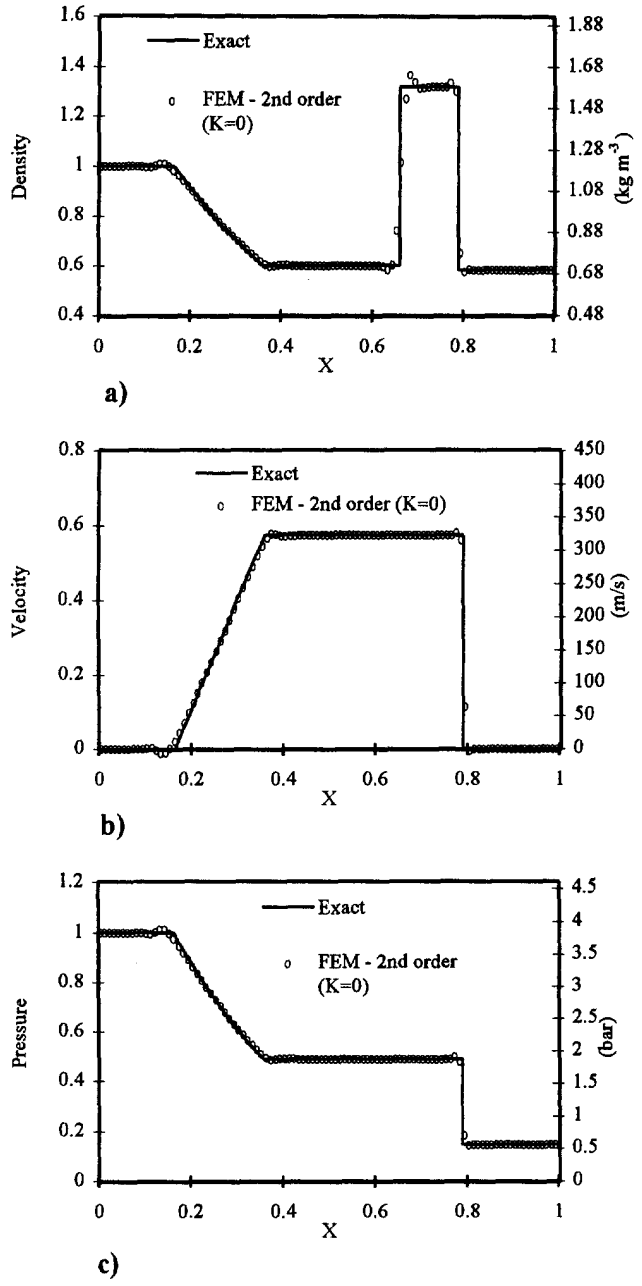

Fig. 5. Results of the shock-tube problem using the discontinuous FEM method, second order, $K = 0$.

The first numerical test is a shock tube problem with the initial conditions considered by Pearson and Winterbone in Ref. [13], contained in Table 1.

In non-dimensional form, the above initial conditions can be transformed in the following way:

$$\mathbf{W}(x,0) = \mathbf{W}^0(x) = \begin{cases} \mathbf{W}_L, & x < 0.5 \\ \mathbf{W}_R, & x \geqslant 0.5 \end{cases} \tag{33}$$

where

$$[\mathbf{W}_L]^T = [\rho_L, (\rho u)_L, (\rho e_0)_L] = [1,\ 0,\ 2.5]$$
$$[\mathbf{W}_R]^T = [\rho_R, (\rho u)_R, (\rho e_0)_R] = [0.5833,\ 0,\ 0.3644] \tag{34}$$

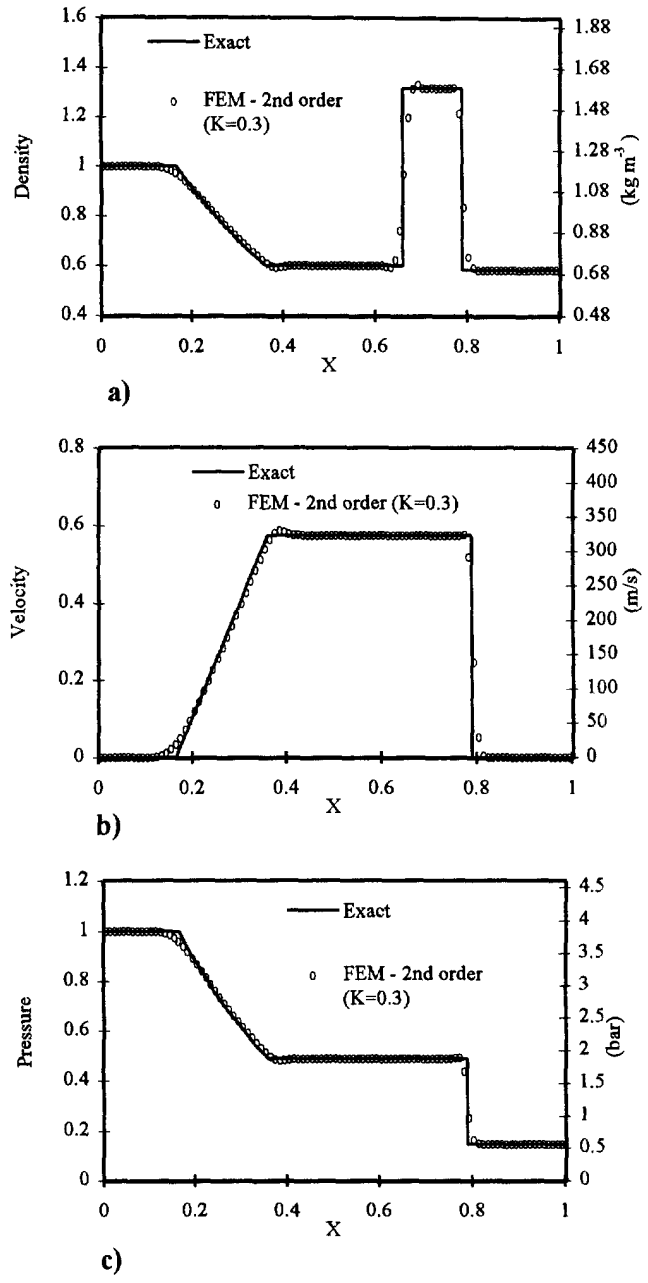

Fig. 6. Results of the shock-tube problem using the FEM method, second order, $K = 0.3$.

Table 1. Initial conditions for the shock-tube problem

	Left state ($x < 0.5$ m)	Right state ($x \geqslant 0.5$ m)
ρ (kg m^{-3})	1.2	0.7
e(MJ Kg^{-1})	0.8	0.2
u(m s^{-1})	0.0	0.0

which have been obtained by assuming the reference state $\rho_{ref} = 1.2$ (kg m^{-3}), $p_{ref} = 384$ (kPa) and a reference length $l_{ref} = 1$ (m), so that the consequent reference time is $t_{ref} = l_{ref}(\rho_{ref}/p_{ref})^{0.5}$.

All the computations were performed using 100 equally spaced elements in the range 0 1. Results at time $t = 0.5$ ms (the corresponding non-dimensional time is $t = 0.28284$) are presented extensively

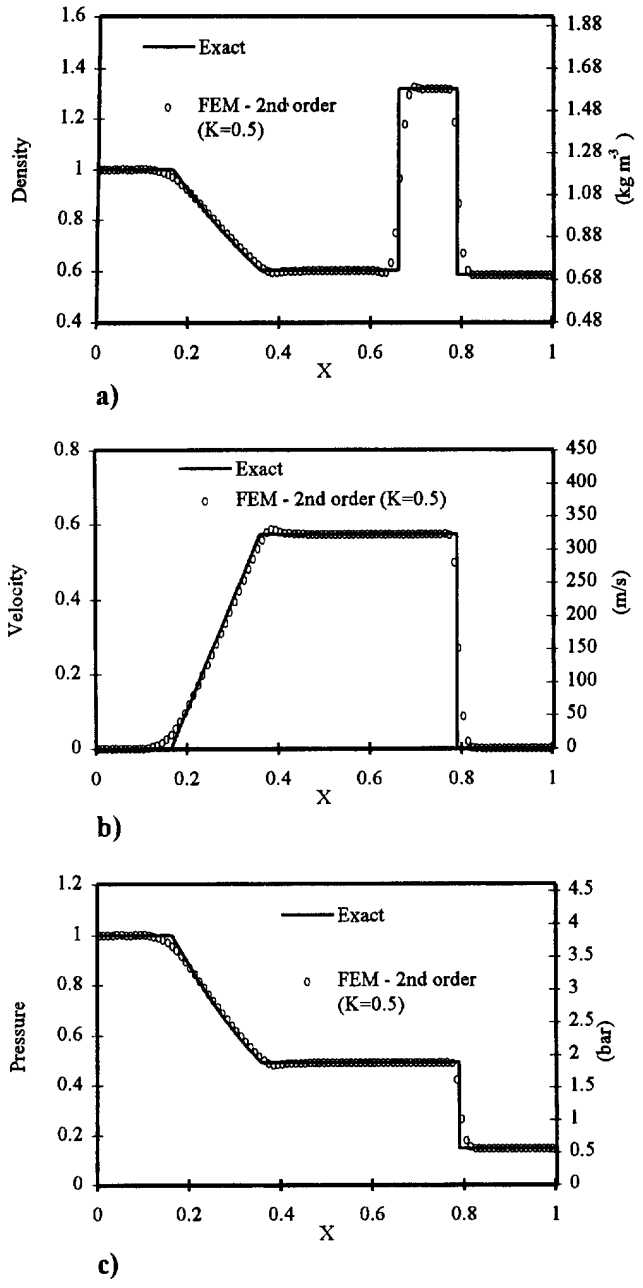

Fig. 7. Results of the shock-tube problem using the FEM method, second order, $K = 0.5$.

in both non-dimensional and dimensional units in Figs 3–10, where the solid lines represent the exact analytical solution. In Table 2 a comparison among absolute and relative CPU times of each method is given.

In all the calculations carried out by LW2 and MCK negligible differences in the results have been pointed out, hence only the LW2 method results are presented in this section.

The spurious oscillations of the numerical solution obtained by the finite difference second-order two-step Lax–Wendroff method are evident near discontinuities. An improvement in the solution can be achieved using the flux corrected transport (FCT) algorithm, even if some wiggles are still present (the results are not reported here, since are fully covered in Ref. [13]). All the oscillations disappear with the total variation diminishing (TVD) algorithm (Fig. 3) but the contact discontinuity and the corners of the rarefaction wave are quite smeared. By adding an artificial compression

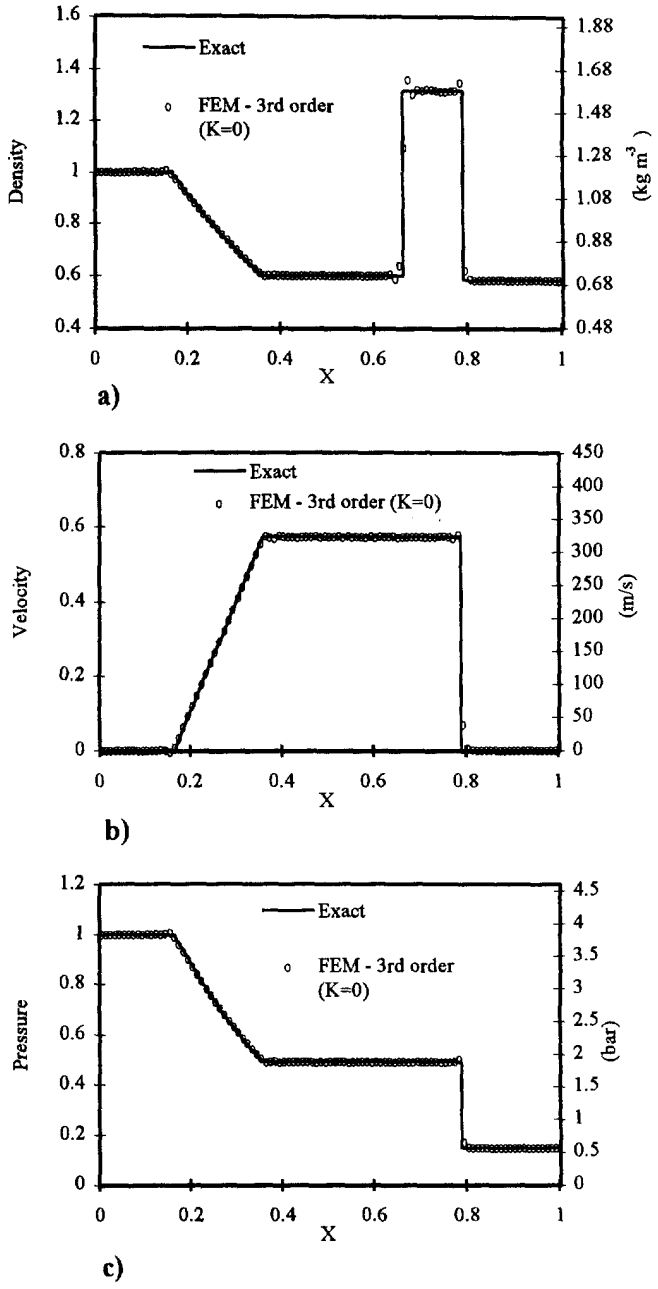

Fig. 8. Results of the shock-tube problem using the FEM method, third order, $K = 0$.

(AC) scheme, the contact discontinuity is captured in few (3–4) elements but the CPU time is almost three times the corresponding value for the simple TVD algorithm (Fig. 4).

Discontinuous finite-element solutions are shown in Figs 5–10. Only the average value within each element was plotted, even if all the Gaussian point values were available. Results from a second-order scheme [i.e. $k = 1$ in Eqn (27)] are presented in Figs 5–7, while the coefficient K increases from 0 to 0.5. The CFL parameter was set to 0.3 in order to allow for convergence. Overshoots and undershoots are significant when $K = 0$. They almost disappear when $K = 0.5$ but the resulting solution is quite smeared, so that an optimum value is K = 0.3. Wiggles are also present when using a third-order scheme ($k = 2$, CFL = 0.2) with quite small values for K but they become negligible for $K = 0.1$ (which therefore can be considered the optimum value): the numerical viscosity is small and the contact discontinuity is correctly captured in 2–3 elements.

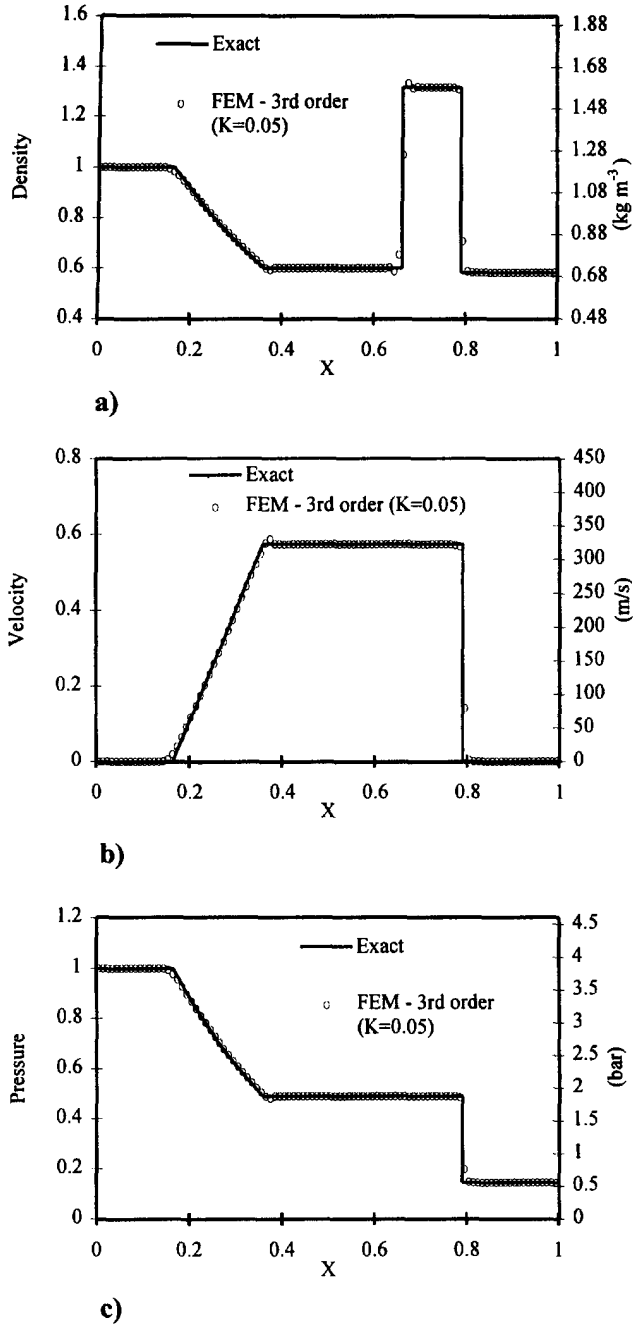

Fig. 9. Results of the shock-tube problem using the FEM method, third order, $K = 0.05$.

The above results show that the coefficient K has to be optimized depending on the order of the scheme. The CPU time for the second-order discontinuous FEM is about 30 times greater than the corresponding one for the LW2 + FCT algorithm, while the accuracy is comparable. Third-order discontinuous finite-element method is about three times more time consuming than the second order one (100 times more than a LW2 + FCT) but results are much more accurate. Notice that the discontinuous FEM code was not optimized and so the computation speed can be considerably increased, according to recent studies [33].

The second test case was chosen according to Refs [14, 17] to highlight the advantages of higher-order methods. We solve the Euler equation (1) with initial conditions:

$$\mathbf{W}(x,0) = \mathbf{W}^0(x) = \begin{cases} \mathbf{W}_L, & x < 0.1 \\ \mathbf{W}_R, & x \geqslant 0.1 \end{cases} \tag{35}$$

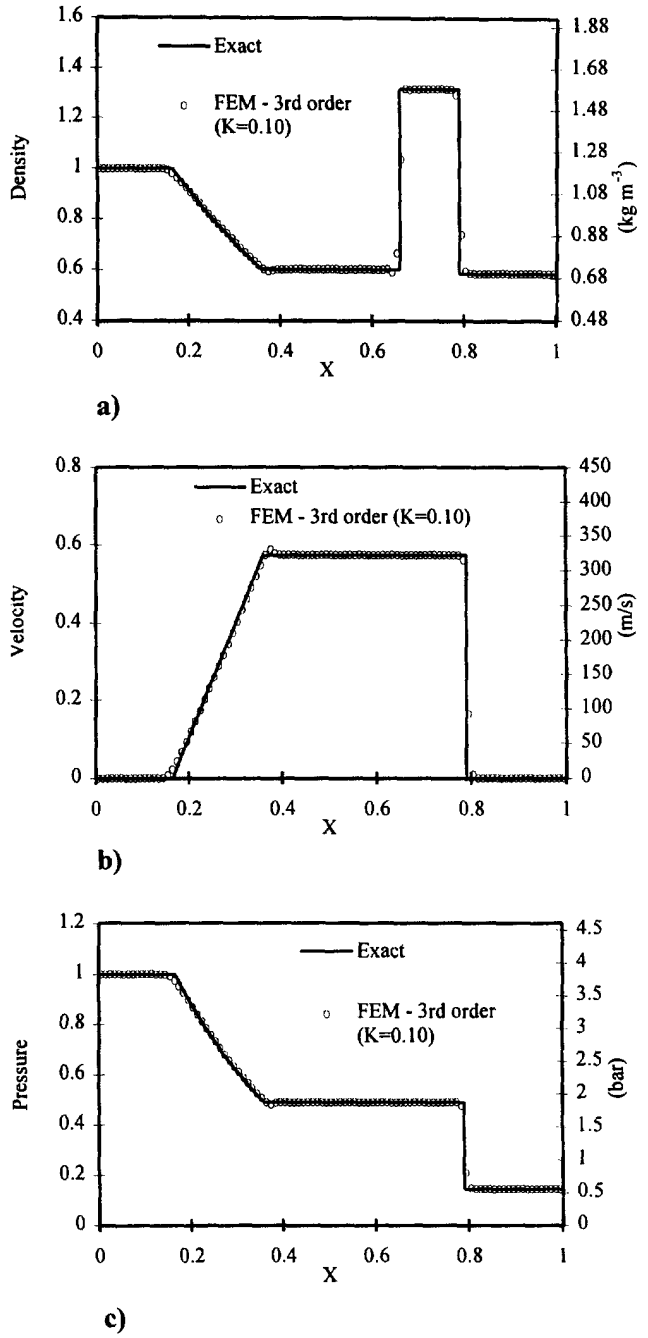

Fig. 10. Results of the shock-tube problem using the FEM method, third order, $K = 0.10$

Table 2. Comparison of CPU times for the shock tube problem (34)

Algorithm	CFL	CPU time (s)	Time factor
LW2	1.0	0.010	0.3
LW2 + FCT smoothing	1.0	0.034	1.0
LW2 + FCT damping	0.866	0.038	1.1
LW2 + TVD	0.7	0.042	1.2
LW2 + TVD + AC	0.7	0.110	3.2
FEM (2nd order)	0.3	1.100	32.3
FEM (3rd order)	0.2	3.600	105.8

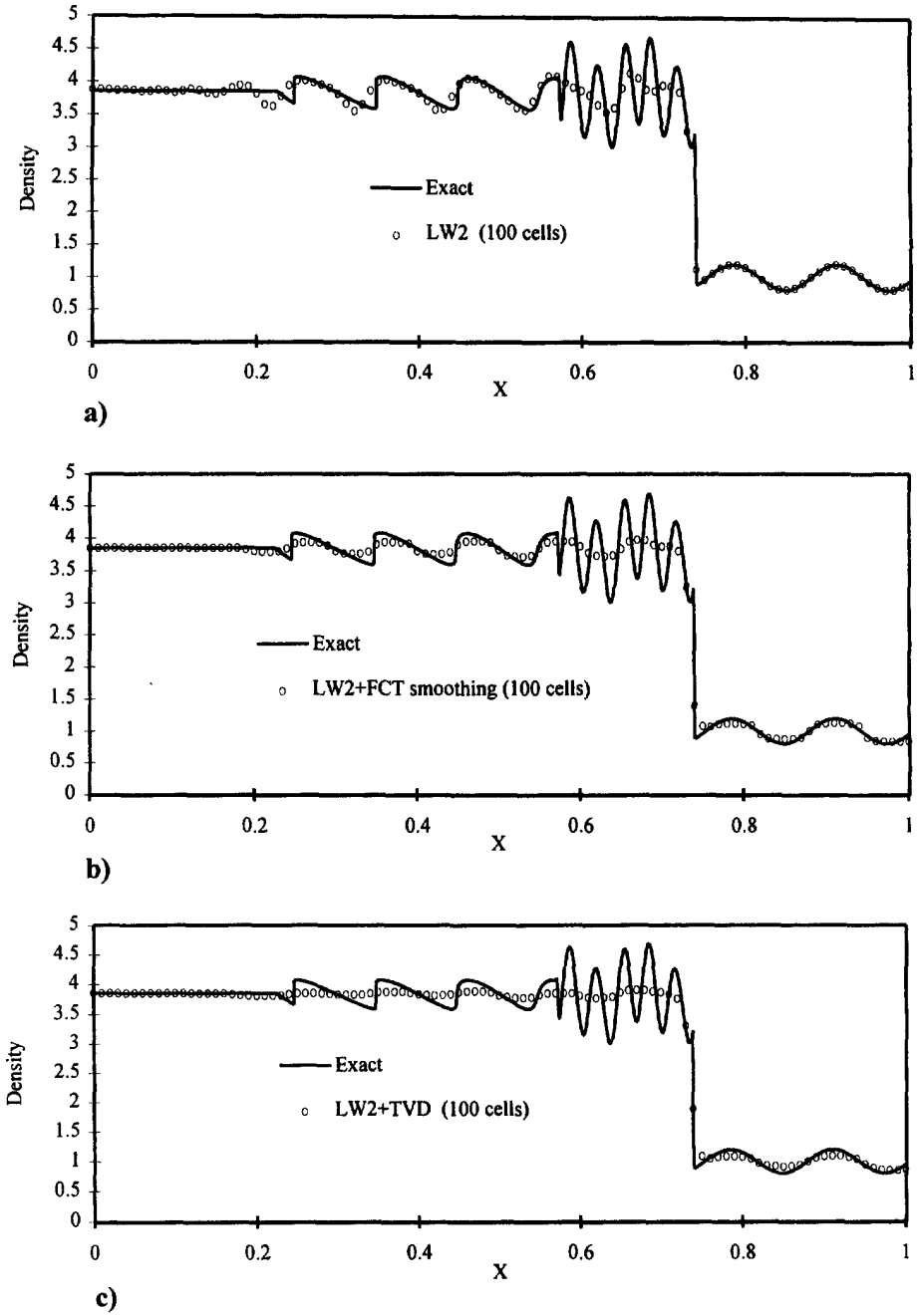

Fig. 11. Results of the shock-turbulence interaction problem using the LW2 (a), LW2 + FCT smoothing (b), LW2 + TVD (c) with 100 cells.

where (in non-dimensional form)

$$[\mathbf{W}_L]^T = [\rho_L, (\rho u)_L, (\rho e_0)_L] = [3.8571,\ 10.1419,\ 39.1668]$$
$$[\mathbf{W}_R]^T = [\rho_R, (\rho u)_R, (\rho e_0)_R] = [1 + 0.2\sin(50x),\ 0,\ 2.5]. \tag{36}$$

This example can be considered a simple model for shock–turbulence interaction [14]. The results at non-dimensional time $t = 0.18$ are shown in Figs 11–16 where the solid line was obtained by the third-order FEM using 1600 elements and should be regarded as the converged (exact) solution. The LW2 gives an oscillating solution near the discontinuities even when 800 equally spaced cells are

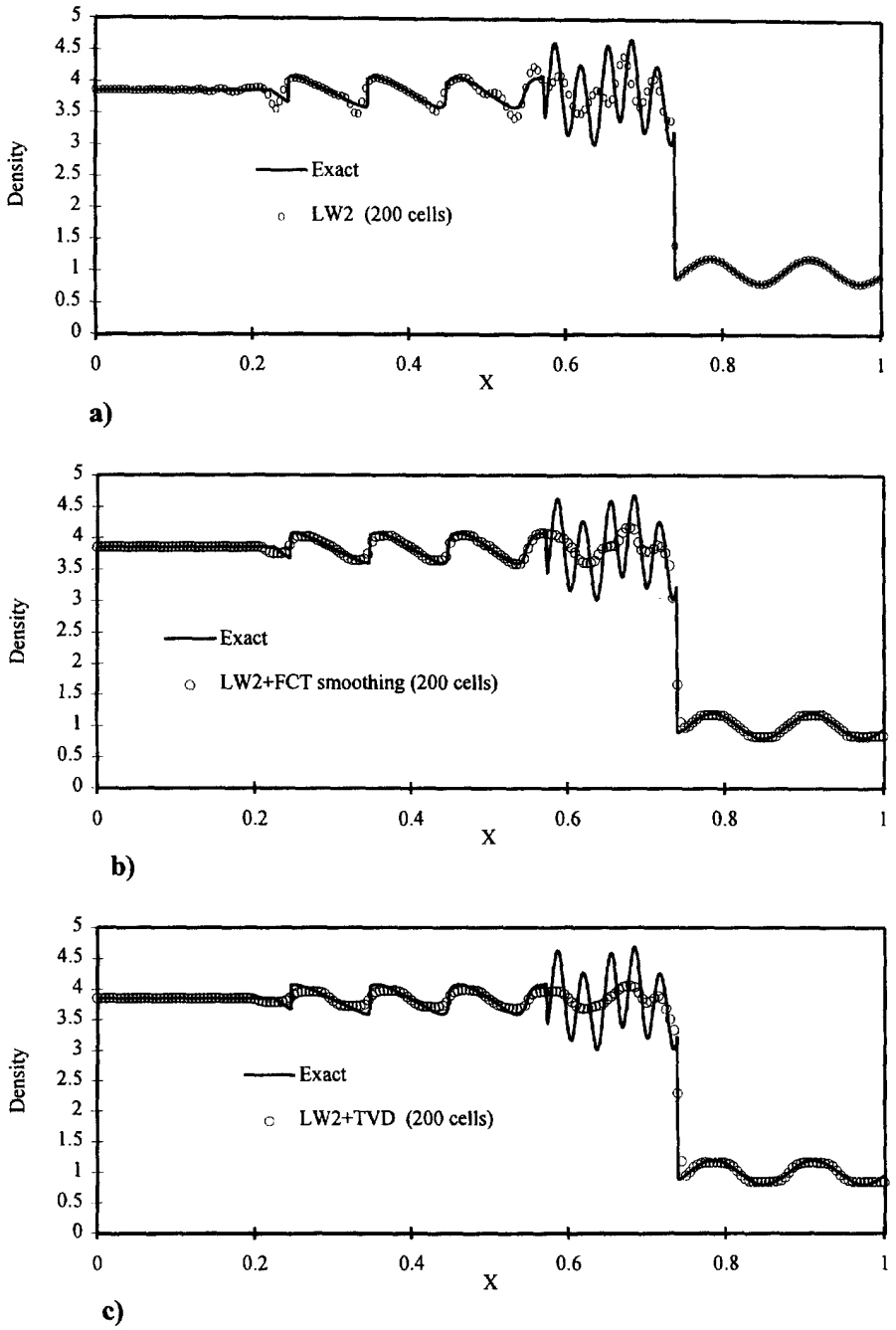

Fig. 12. Results of the shock-turbulence interaction problem using the LW2 (a), LW2 + FCT smoothing (b), LW2 + TVD (c) with 200 cells.

considered (Fig. 14(a)), because of the high numerical dispersion introduced. Due to the switching to a first-order scheme near points of extrema even in smooth regions, the LW2 + TVD algorithm excessively smears the solution [Figs 11(c), 12(c), 13(c), 14(c)]. The improvement obtained through a LW2 + TVD + AC scheme, limited to the discontinuity region, is negligible and so is not presented here. It may be noted that the LW2 + FCT via smoothing performs better in the smooth regions of the solution (it is not TVD), introducing a diffusion smaller than LW2 + TVD. The second-order discontinuous FEM performs quite well when using 400 elements at least with K set to the optimum value of 0.3 [Fig. 15(c)], whilst the solution with the 100 element grid [Fig. 15(a)] is unsatisfactory and similar to the corresponding LW2 solution of Fig. 11(a). Here, as above only one

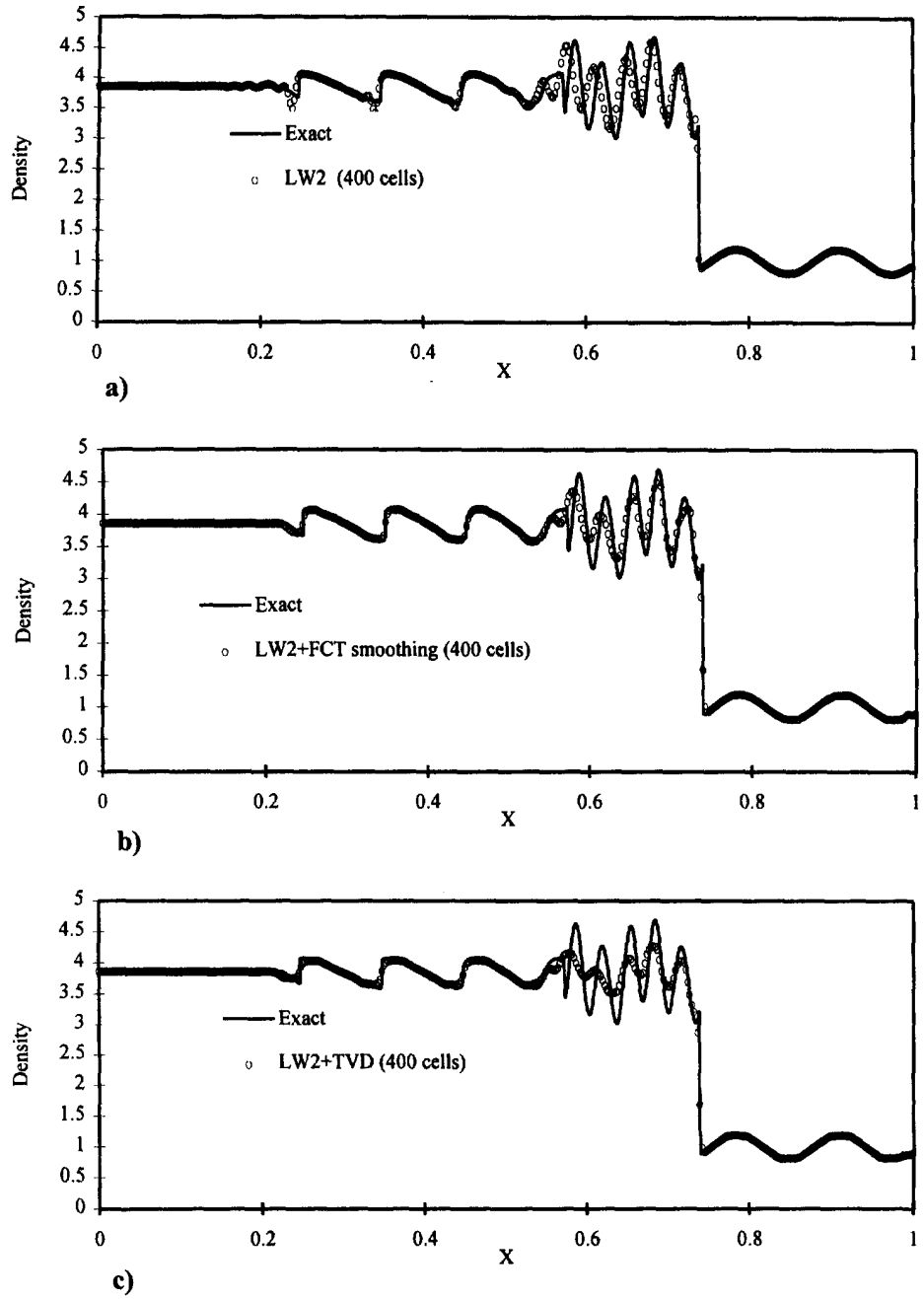

Fig. 13. Results of the shock-turbulence interaction problem using the LW2 (a), LW2 + FCT smoothing (b), LW2 + TVD (c) with 400 cells.

point per element was plotted. It may be observed that the solution obtained by LW2 + FCT(or + TVD) on a 800 cell grid [Fig. 14(b)] is comparable to that given by the third-order FEM on a coarser mesh with only 200 elements (Fig. 16(b), $K = 0.1$). Moreover, the third-order FEM provides a good solution even with 100 elements [Fig. 16(a)].

Time factors are similar to those shown in Table 1 and vary quadratically with the number of elements. The comparison of the computer times needed to solve the shock-tube problem on a given grid shows that the finite difference schemes are faster than the second- and third-order FEM by a factor of about 30 and 100, respectively. However, a comparison between the results of the shock–turbulence interaction problem shows that LW2 + FCT(or + TVD) on the 400 element grid

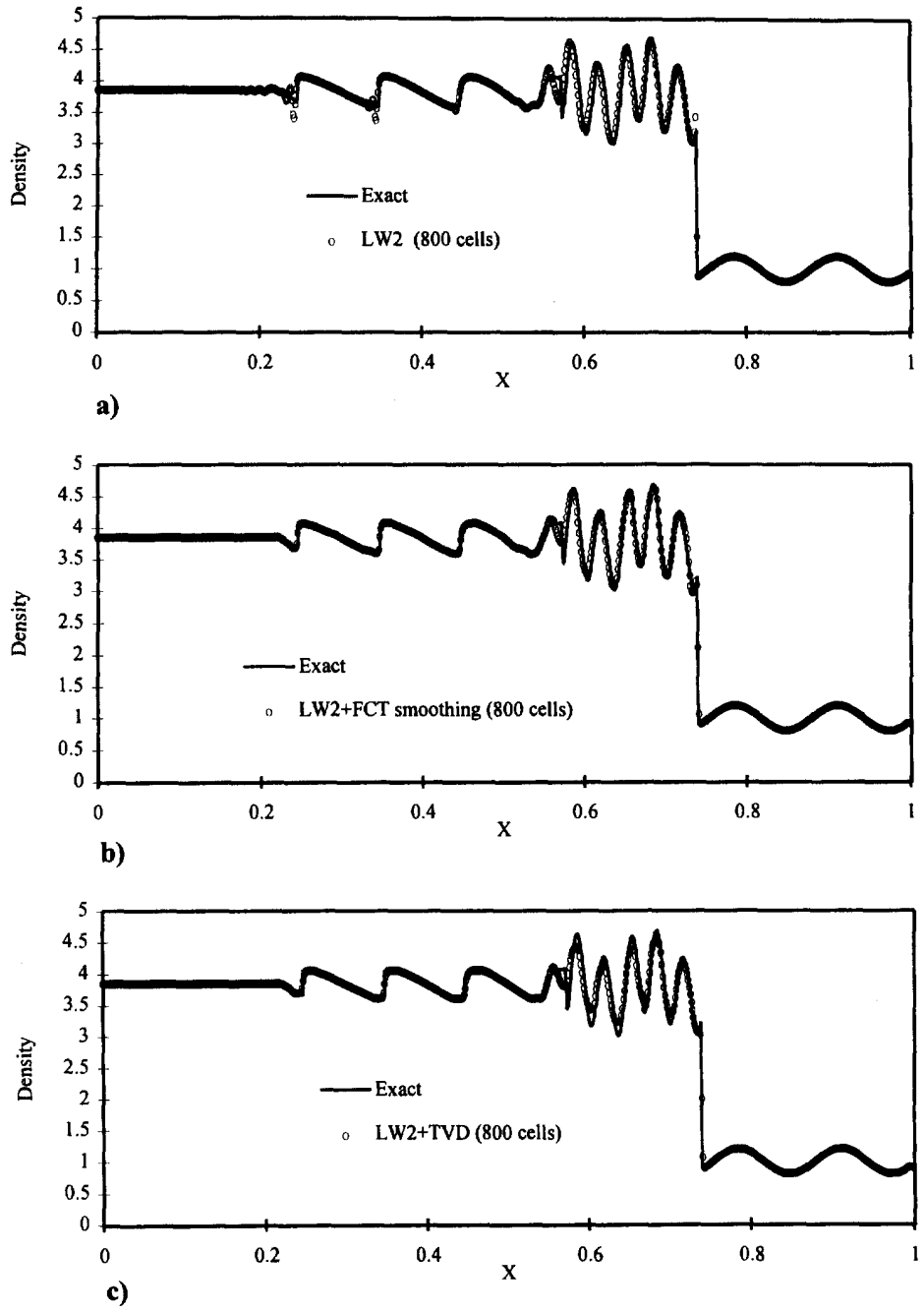

Fig. 14. Results of the shock-turbulence interaction problem using the LW2 (a), LW2 + FCT smoothing (b), LW2 + TVD (c) with 800 cells.

[Fig. 13(b) and (c)] is slightly less accurate than the second-order FEM on the 200 element grid [Fig. 15(b)]. As a consequence, if we compare solutions with similar accuracy, the LW2 + FCT is faster than the second-order FEM by a factor which is less than 30/4, since, due to the halved time step and mesh size, four times as much computer time is needed when passing from a 200 to a 400 element grid.

Since the third-order FEM solution on the 200 grid displays about the same accuracy as the LW2 + FCT solution on the 800 grid, the previous observation implies that the LW2 + FCT is faster than the third-order FEM by a factor which is less than 100/16, if the same accuracy is required.

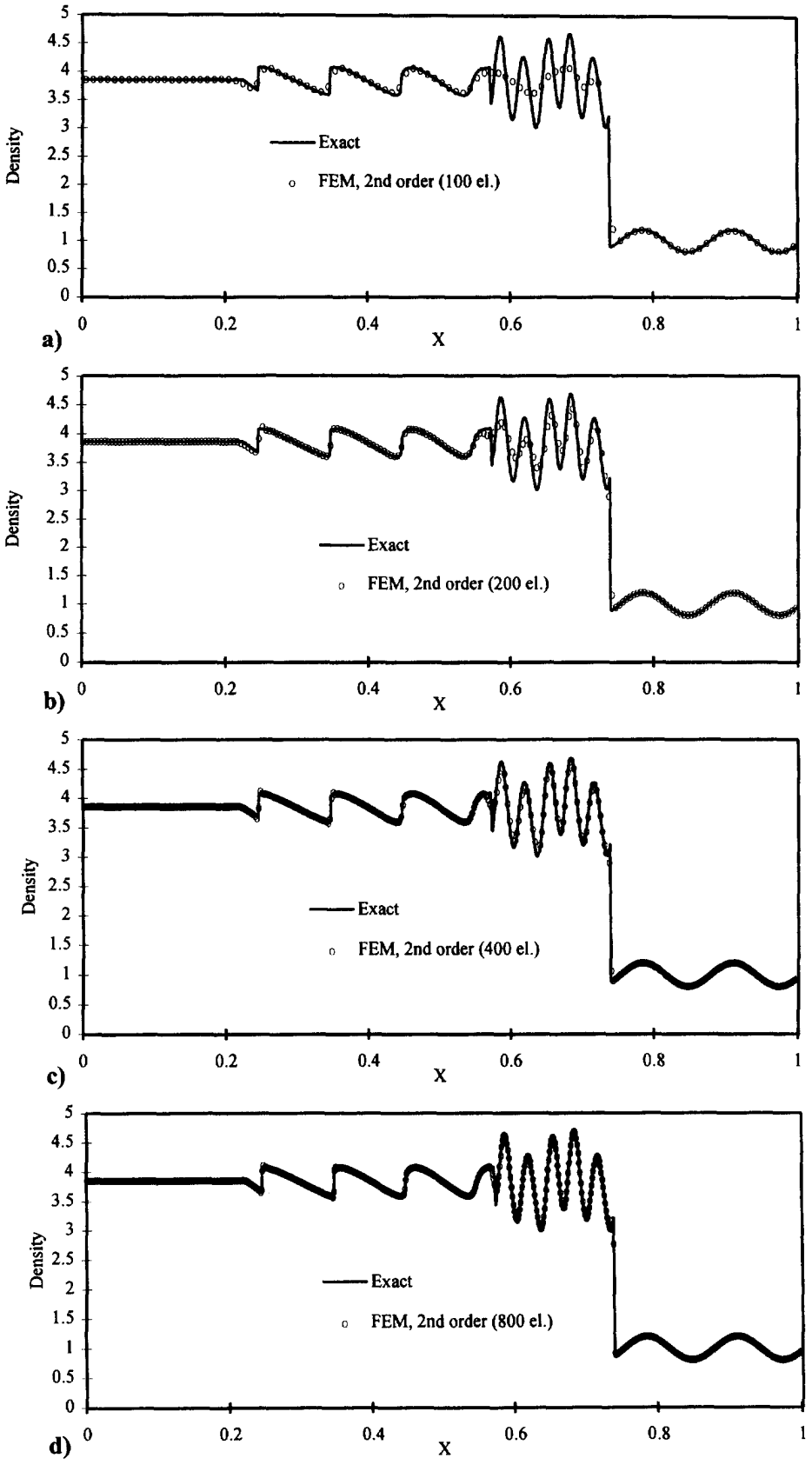

Fig. 15. Results of the shock-turbulence interaction problem using the second-order FEM with 100 (a), 200 (b), 400 (c), 800 (d) elements.

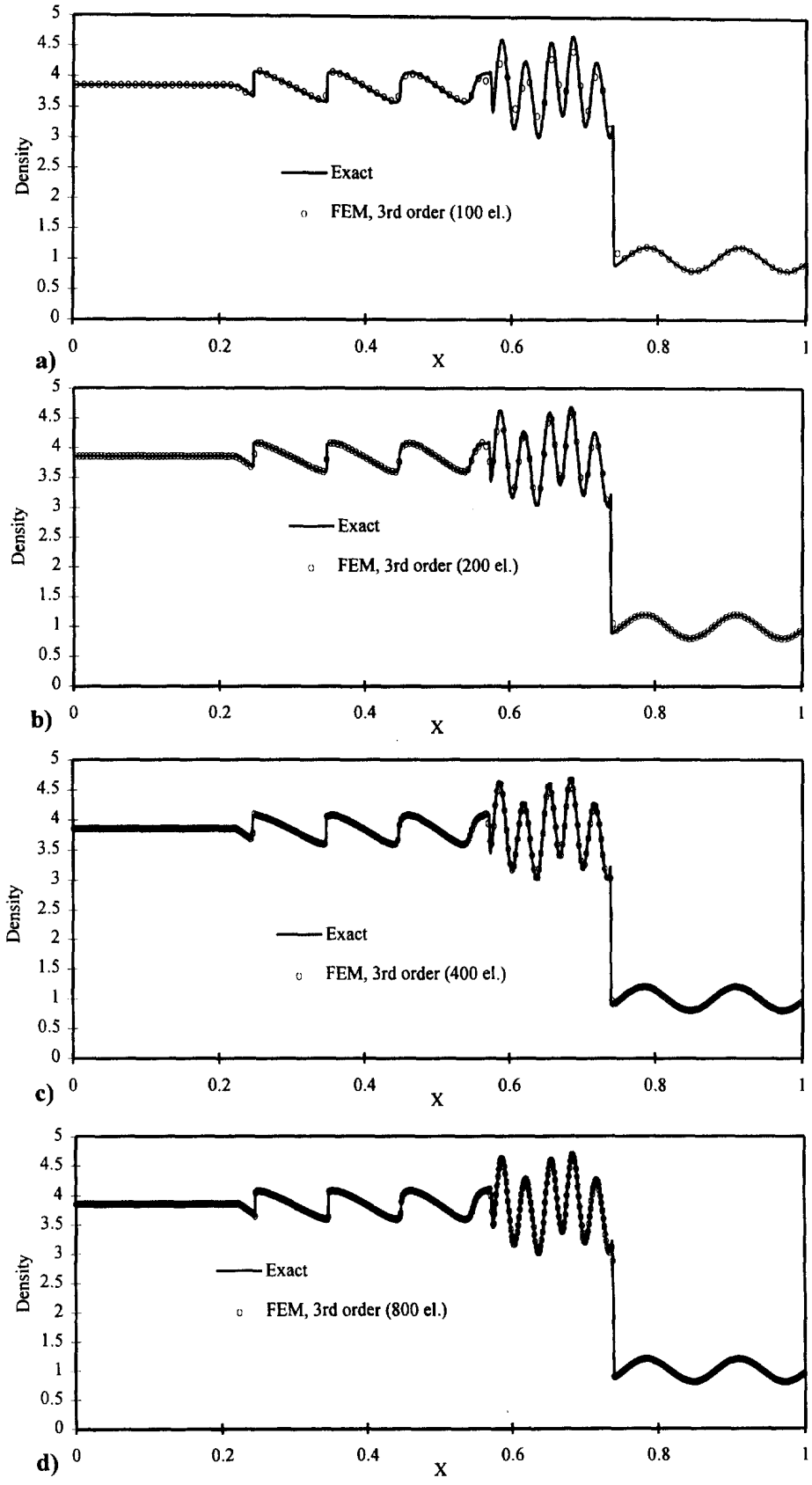

Fig. 16. Results of the shock-turbulence interaction problem using the third-order FEM with 100 (a), 200 (b), 400 (c), 800 (d) elements.

5. CONCLUSIONS

In this work we have compared the results obtained with symmetric finite difference schemes and with a discontinuous finite-element method in the solution of classical test cases for one-dimensional unsteady flows in ducts. We have considered the second-order accurate two-step Lax–Wendroff method and the MacCormack predictor–corrector method with the addition of the FCT or the TVD techniques, and a second- and third-order accurate discontinuous Galerkin finite-element method.

The shock-tube calculations show that the second-order accurate finite-difference and finite-element results have a very similar accuracy, whilst the third-order accurate FEM gives significant improvements in the resolution of the discontinuities.

If we consider the shock–turbulence interaction problem, in which the solution is characterized by shocks as well as by high-frequency oscillations, the gain in accuracy of the third-order FEM is more evident, especially if we compare the results obtained with the 100 element mesh.

As discussed in the previous section, the FEM is computationally more demanding than finite-difference schemes. However, a significant improvement should be obtained by adopting the implementation suggested in Ref. [33].

In addition, the FEM is well suited to model flow regions characterized by strong variation of the cross-sectional area and of friction and heat transfer at duct walls, since this method allows a more flexible local refinement of the mesh, so that adjacent ducts with very different mesh size may be easily treated. Moreover, hybrid FEM models coupling 1D calculations of flows in ducts with 3D direct modelling of flow boundary regions could be naturally developed. In fact, the greater geometrical flexibility and the straightforward treatment of boundary conditions allowed by the FEM could be crucial advantage in these cases over the more commonly adopted finite-difference techniques. This is especially true in multidimensional applications since the FEM is ideally suited to be used on unstructured grids.

In the future, we plan to exploit the potential of the FEM by modelling more complex unsteady flows such as those arising in realistic i.e. engine intake and exhaust configurations.

REFERENCES

1. Benson, R. S., Garg, R. D. and Woollatt, D., A numerical solution of unsteady flow problems. *International Journal of Mechanical Sciences*, 1964, **6**, 17–144.
2. Benson, R. S., The thermodynamics and gas dynamics of internal combustion engines. In eds. J. H. Horlock and D. E. Winterbone. Clarendon Press, Oxford, 1982.
3. Blair, G. P. and Goulburn, J. R., The pressure-time history in the exhaust system of a high speed reciprocating internal combustion engine. *SAE Transactions*, 1967, **76**, paper n. 670477.
4. Poloni, M., Winterbone, D. E. and Nichols, J. R., Calculation of pressure and temperature discontinuity in a pipe by the method of characteristics and the two-step differential Lax–Wendroff method. *International Symposium on Flows in Internal Combustion Engines, FED*, **62**, ASME Annual Winter Meeting, Boston 1987.
5. Onorati, A., Winterbone, D. E. and Pearson, R. J., A comparison of the Lax-Wendroff technique and the method of characteristics for engine gas dynamic calculations using fast Fourier transform spectral analysis. *SAE International Congress & Experiments* (Detroit, Michigan), paper no. 9302428, 1993.
6. Ferrari, G. and Onorati, A., Determination of silencer performances and radiated noise spectrum by 1-d gas dynamic modelling. *XXV FISITA Congress* (Beijing, China), paper no. 945135, 1994.
7. Giannattasio, P. and Dadone, A., Applications of a high resolution shock-capturing scheme to the unsteady flow computation in engine ducts. In *Proceedings Institute of Mechanical Engineers Conference on Computers in Engine Technology*. Cambridge, U.K., 1991, pp. 119–126.
8. Boris, J. P. and Book, D. L., Flux-corrected transport, I. Shasta, a fluid transport algorithm that works. *Journal of Computational Physics*, 1973, **11**, 38–69.
9. Book, D. L., Boris, J. P. and Hain, K., Flux-corrected transport, II. Generalisations of the method. *Journal of Computational Physics*, 1975, **18**, 248–283.
10. Niessner, H. and Bulaty, T., A family of flux-correction methods to avoid overshoot occurring with solutions of unsteady flow problems. In *Proceedings of the 4th GAMM Conference on Numerical Methods and Fluid. Mechanics*, 1981 Paris, pp. 241–250.
11. Davis, S., TVD finite-difference schemes and artificial viscosity. **NASA CR** 1984, 172373.
12. Winterbone, D. E. and Pearson, R. J., A Solution of the wave equations using real gases. *International Journal of Mechanical Sciences*, 1992, **34**, 917–932.
13. Pearson, R. J. and Winterbone, D. E., Calculating the effects of variations in composition on wave propagation in gases. *International Journal of Mechanical Scienes*, 1993, **35**, 517–537.
14. Shu, C. and Osher, S., Efficient implementation of essentially non-oscillatory shock-capturing schemes, II, *Journal Computational Physics*, 1989, **83**, 32–78.

15. Saurel, R., Larini, M. and Loraud, J. C., Exact and approximate Riemann solvers for real gases. *Journal of Computational Physics* 1994, **112**, 126–137.
16. Cockburn, B. and Shu, C. W., TVB Runge–Kutta local projection discontinuous Galerkin finite element method for conservation laws II: general framework. *Mathematics of Computation*, 1989, **52**, 411–435.
17. Cockburn, B. and Shu, C. W., TVB Runge–Kutta local projection discontinuous Galerkin finite element method for conservation laws III: one dimensional systems. *Journal of Computational Physics*, 1989, **84**, 90–113.
18. Hirsh, C., Numerical computation of internal and external flows, Vol I–II. Wiley, New York 1991.
19. Winterbone, D. E., Pearson, R. J. and Zhao, Y., Numerical simulation of intake and exhaust flows in a high speed multi-cylinder petrol engine using the Lax–Wendroff method. In *Proceedings of the Institute of Mechanical Engineers Conference on Computers in Engine Technology*, Cambridge, U.K., 1991, pp. 91–99.
20. Bulaty, T. and Niessner, H., Calculatioin of 1-D unsteady flows in pipe system of i.c. engines. American Society of Mechanical Engineers *Journal Fluid Engineering*, 1986, **107**, 407–412.
21. Chang, S. and To, W., A brief description of a new numerical framework for solving conservation laws — the method of space–time conservation element and solution element. **NASA** Technical Memorandum 1992, 105757.
22. Briz, G. and Giannattasio, P., Applicazione dello schema numerico conservation element - solution element al calcolo del flusso intazionario nei condotti dei motori a c.i. In *Proceedings of the 48th ATI National Congress*, Taormina, Italy, 1993, pp. 233–247.
23. Onorati, A., Numerical simulation of exhaust flows and tailpipe noise of a small single cylinder Diesel engine, In *Proceedings of the Small Engine Technology Conferences SETC '95*, SAE paper No. 951755, 1995, pp. 1–11. Milwaukee, WI.
24. Ikeda, T. and Nakagawa, T., On the SHASTA FCT algorithm for the equation $\partial\rho/\partial t + \partial[v(\rho)\rho]/\partial x = 0$. *Mathematics of Computation*, 1979, **33** 1157–1169.
25. Harten, A., The artificial compression method for computation of shocks and contact discontinuities: III. Self-adjusting hybrid schemes, *Mathematics of Computation*, 1978, **32** 363–389.
26. Lesaint, P., Sur la résolution des systèmes hyperboliques du premier ordre par des méthodes d'éléments finis. Ph.D thesis, Université Paris 6, 1975.
27. Lesaint, P. and Raviart, P. A., On a finite element method to solve the neutron transport equation. In *Mathematical Aspects of Finite Elements in Partial Differential Equations*, ed. C. De Boor Academic Press, 1974, pp. 89–145.
28. Bassi, F., Rebay, S. and Savini, M., A high resolution discontinuous Galerkin method for hyperbolic problems on unstructured grids. In proceedings of 3rd International Conference on Fluid Dynamics, Reading, *Numerical Methods in Fluid Dynamics*, ed. K. W. Morton and M. J. Baines. Clarendon Press, Oxford, 1993, pp. 345–354.
29. Bassi, F., Rebay, S. and Savini, M., Discontinuous finite element Euler solutions on unstructured adaptive grids. In proceedings of 3rd International Conference on Numerical Methods in Fluid Dynamics, Rome, *Lecture Notes in Physics*, ed. by M. Napolitano and E. Sabetta, Vol. 414. Springer, Berlin, 1993, pp. 245–249.
30. Bassi, F. and Rebay, S., Accurate 2D Euler computations by means of a high order discontinuous finite element method. In proceedings of 14th International Conference on Numerical Methods in Fluid Dynamics,Bangalore, in *Lecture Notes in Physics*, Springer, Berlin, 1994.
31. Bassi, F. and Rebay, S., Discontinuous finite element high order accurate numerical solution of the compressible Navier-Stokes equations. In proceedings of 4th International Conference on Fluid Dynamics, Oxford, *Numerical Methods in Fluid Dynamics*, eds M. J. Baines and K. W. Morton. Clarendon Press, Oxford, U.K., 1995.
32. Johnson, C., Numerical Solution of Partial Differential Equations by the Finite Element Method. Combridge University Press, Cambridge, U.K., 1987.
33. Gregoire, J. P. and Pot, G., Speedup of CFD codes using analytical FE calculations. In proceedings of 14th International Conference on Numerical Methods in Fluid Dynamics., Bangalore, *Lecture Notes in Physics*. Springer, Berlin, 1994.